Draft version August 29, 2019
Typeset using LaTeX **twocolumn** style in AASTeX61

BAFFLES: BAYESIAN AGES FOR FIELD LOWER-MASS STARS

S Adam Stanford-Moore,[1] Eric L. Nielsen,[1] Robert J. De Rosa,[1] and Bruce Macintosh[1]

[1] *Kavli Institute for Particle Astrophysics and Cosmology, Stanford University, Stanford, CA 94305, USA*

ABSTRACT

Age is a fundamental parameter of stars, yet in many cases ages of individual stars are presented without robust estimates of the uncertainty. We have developed a Bayesian framework, `BAFFLES`, to produce the age posterior for a star from its calcium emission strength ($\log(R'_{HK})$) or lithium abundance (Li EW) and $B-V$ color. We empirically determine the likelihood functions for calcium and lithium as functions of age from literature measurements of stars in benchmark clusters with well-determined ages. We use a uniform prior on age which reflects a uniform star formation rate. The age posteriors we derive for several test cases are consistent with literature ages found from other methods. `BAFFLES` represents a robust method to determine the age posterior probability distribution for any field star with $0.45 \leq B-V \leq 0.9$ and a measurement of R'_{HK} and/or $0.35 \leq B-V \leq 1.9$ and measured Li EW. We compile colors, R'_{HK}, and Li EW from over 2630 nearby field stars from the literature and present the derived `BAFFLES` age posterior for each star.

Keywords: Stellar activity (1580), Stellar ages (1581), Field stars (2103), Bayes' Theorem (1924), Bayesian statistics (1900)

Corresponding author: S Adam Stanford-Moore
sasm@stanford.edu

1. INTRODUCTION

Age, along with mass and metallicity, is a fundamental parameter of stars. Accurate stellar ages are needed in a wide variety of astronomical studies, from galactic evolution, globular clusters, open clusters, star forming regions, stellar multiples, brown dwarf companions, and planetary systems. For direct imaging exoplanet surveys, such as the Gemini Planet Imager Exoplanet Survey (Macintosh et al. 2018; Nielsen et al. 2019), stellar age is important at all stages of the survey. First, while selecting target stars, younger stars are preferred, since their planets will be inherently brighter and easier to detect. Second, the mass for an imaged planet is derived from the age of the host star using evolutionary models that link mass, age, and luminosity (e.g. Allard 2014; Baraffe et al. 2015), and the dominant measurement uncertainty in deriving mass is from age (Bowler 2016). Third, age is a requirement for measuring the occurrence rates of planets. Translating sensitivity in apparent brightness to mass sensitivity requires the age of each observed star. Thus completeness to planets as a function of mass, a key ingredient for occurrence rate, relies heavily on precise ages for the entire sample (e.g. Bowler 2016; Nielsen et al. 2013, 2019).

Yet unlike the ages of stars in co-eval groups, like open clusters or moving groups, the ages of field stars are difficult to determine robustly. For stellar clusters with well-determined membership lists, the main sequence turnoff is used to robustly determine the age (e.g. Goudfrooij et al. 2014; Cummings & Kalirai 2018). The lithium depletion boundary is applicable to both clusters and more sparse moving groups, with the reddest objects in an association with detectable lithium absorption setting the overall age (e.g. Burke et al. 2004; Soderblom 2010). For isolated field stars, however, a less robust set of observables that track age are available, including spectroscopic indicators (e.g. Skumanich 1971; Wright et al. 2004), gyrochronology (e.g. Kraft 1967; Barnes 2009), and asteroseismology (e.g. Cunha et al. 2007). Here we present a Bayesian method to determine age through two spectral indicators: calcium emission strength and the depth of the lithium absorption line.

1.1. *Empirical Age Indicators*

1.1.1. *Calcium Emission Strength*

Calcium emission strength, as given by the index R'_{HK}, is connected to the strength of a star's magnetic field through the stellar dynamo (Noyes et al. 1984). The rotation of the star and convection within induces a magnetic field whose strength is proportional to the rate of rotation (Noyes et al. 1984; Skumanich 1971). Over time the star's rotation inevitably slows as it ejects ionized particles in its stellar wind, which carry away angular momentum (Kraft 1967; Weber & Davis 1967), and as a result the magnetic field strength and thus calcium emission strength generally decrease with age.

The index R'_{HK} is a measure of the flux in the narrow emission line in the core of the Calcium II H and K absorption lines at ∼3968 Å and ∼3934 Å respectively (Noyes et al. 1984; Wright et al. 2004). R'_{HK} is derived from an intermediate index, the S index, which represents the ratio of the narrow emission flux to the background continuum flux. S provides a relative comparison of emission strength, yet includes both chromospheric and photospheric contributions and is dependent on $B-V$ (as well as age). Therefore, to remove the dependencies on $B-V$ the S index is transformed by two empirically determined polynomials in $B-V$, resulting in R'_{HK} (Noyes et al. 1984; Wright et al. 2004), where the polynomials have been calibrated over a $B-V$ range of 0.45 to 0.90, corresponding to an approximate spectral type range of F6 to K2. In addition to the long-term decline in activity over time, the S value for a single star also varies by ∼10% over that star's activity cycle (Wright et al. 2004).

1.1.2. *Lithium Equivalent Width*

The strength of the lithium absorption line traces the amount of lithium present in the photosphere of a star. When stars initially form their primordial lithium abundance is similar to the abundance from Big Bang nucleosynthesis, with number density of $\sim 10^{-9}$ that of hydrogen (Sestito & Randich 2005). Over time stars deplete their primordial lithium by nuclear burning in the core and convective mixing, so that measurements of remaining surface lithium correlate with stellar age (Soderblom 2010; Skumanich 1971). For stars cooler than ∼7000 K, lithium abundance can be measured based on the equivalent width (EW) of the absorption of the lithium doublet at 6708 Å (Soderblom 2010); hotter stars (OBA spectral types) have ionized their lithium, and have negligible 6708 Å absorption even with no lithium burning.

Lithium's two isotopes, ^{6}Li and the more abundant ^{7}Li, burn at temperatures of 2.2 million K and 2.6 million K, respectively. Since stellar surface temperatures are much lower (∼2500 K for low-mass M stars and ∼46000 K for high-mass O-stars), in order to burn, lithium must be brought into hotter layers via convection (Soderblom et al. 1990). As a result, the rate of lithium depletion largely depends on the depth of the convection zone, allowing lower-mass stars – which while having lower surface temperatures have much deeper convective layers – to deplete lithium faster than higher-mass stars (Soderblom et al. 1990). In addition to con-

vection it is thought that slow mixing induced by rotation and angular momentum loss may affect lithium depletion (Sestito & Randich 2005), so that lithium abundance is a function of age, spectral type, and the initial rotation rate and rotational evolution of the star.

1.2. *Functional fits to R'_{HK} and Li EW evolution*

Previous studies have taken advantage of the correlation between R'_{HK} and age to create empirical fits of mean cluster $\log(R'_{HK})$ vs. log cluster age (Soderblom et al. 1991; Donahue 1993; Lachaume et al. 1999; Mamajek & Hillenbrand 2008). However while these polynomial fits allow one to find an expression for age as a function of R'_{HK}, the polynomial makes no direct prediction of uncertainty in the age derivation. Soderblom et al. (1991) found the standard deviation of their stellar data around their power-law fit to be $\sim$0.2 dex and concluded that ages predicted from their fit would be accurate to $\sim$50%. A similar approach has been done for lithium as well (finding an average fit to clusters, and assigning a single age to a star based on its location relative to the cluster fits), e.g. Mamajek et al. 2002; Nielsen & Close 2010. However this method fails to capture the full astrophysical scatter.

In addition, many polynomial fits fail to account for a uniform star formation rate in the Milky Way (with exceptions such as the second polynomial fit developed by Soderblom et al. (1991)). $\mathrm{Log}(R'_{HK})$ changes roughly uniformly in log age and as a result, most fits are done in log(age). A uniform star formation rate translates to a prior in log(age) that increases the likelihood of older ages. Therefore polynomial fits to cluster means without this prior tend to underestimate stellar ages of observed stars.

Furthermore, the median age estimates for separate methods (e.g. R'_{HK} and Li EW) are difficult to rigorously combine without precise uncertainty estimates. Previous works have, for example, simply averaged the ages obtained from R'_{HK} and lithium e.g. Nielsen & Close 2010.

Brandt et al. (2014b) develops a Bayesian method to combine the age PDF of a star's likely moving group with its posterior PDF from indicators of chromospheric and X-ray activity and stellar rotation. The two age distributions are then averaged, weighted by the probability of membership to the moving group. Other works (e.g. Casagrande et al. 2011,Nielsen et al. 2013) have developed Bayesian methods for deriving age posteriors from isochrones that also utilize a uniform star formation rate prior.

We describe here a method to derive Bayesian ages for field stars from lithium or calcium measurements, Bayesian Ages For Field LowEr-mass Stars (`BAFFLES`).[1] For calcium emission our method is calibrated to stars with $B-V$ between 0.45 and 0.9 ($\sim$F6–K2) and $\log(R'_{HK})$ between -3.7 and -5. For lithium we have calibrated `BAFFLES` to stars with $B-V$ between 0.35 and 1.9 ($\sim$F2-M5) and Li EW between 3.2 and 1500 mÅ.

2. DATA

We calibrate `BAFFLES` using benchmark moving groups and open clusters with well-determined ages. While calcium emission strength and lithium abundance serve as indicators of relative age, we use these clusters to calibrate the relationships that give age as a function of indicator. Table 1 gives basic properties on each benchmark cluster as well as our assumed age for each.

Since the ages of the benchmark clusters anchor the calcium and lithium age relations, accurate ages are important to the accuracy of `BAFFLES`; the offset in the posteriors scales with the factor by which the ages are modified. For both lithium and calcium, modifying the age of a single cluster by $\pm1\sigma$, tends to change the median age derived by `BAFFLES` by $\lesssim 3\%$. Systematically shifting all the cluster ages in the same direction by $\pm1\sigma$ shifts the derived median ages of posteriors by a comparable amount, $\lesssim 20\%$.

2.1. *Calcium benchmark clusters*

Ages, stellar R'_{HK} values, and stellar $B-V$ values used in this work for calcium were compiled by Mamajek & Hillenbrand (2008), though here separately reported measurements for the same star are averaged together (though this had little effect on our fits). Adopted ages for the benchmark clusters were mostly identical to those adopted by Mamajek & Hillenbrand (2008), except we used more recent age estimates of 24 Myr for β Pic and 45 Myr for Tuc/Hor from Bell et al. (2015), 10 Myr for Upper Scorpius from Pecaut & Mamajek (2016), and $\sim$700 Myr for Hyades from Brandt & Huang (2015); Gossage et al. (2018).

2.2. *Lithium benchmark clusters*

We compiled $B-V$ and Li EW measurements from the multiple sources listed in Table 1. For duplicate stars we averaged measurements, and use the measurement if there was one measurement and one upper limit.

[1] Our `BAFFLES` package is available at https://github.com/adamstanfordmoore/BAFFLES and can be used from the command line with *python baffles.py -bmv [B-V] -rhk [Log(R'_{HK})] -li [Li EW]* (with other options available).

Group Name	Age (Myr)	Age Ref.	$N_{\rm Ca}$	Ca Ref.	$N_{\rm Li}$	Li Ref.
NGC2264	5.5	3			123	9,10
Upper Scorpius	10	20	8	1		
UCL+LCC	16	21,22	8	1		
β Pic	24	2	6	1,30,31	37	14,19
IC2602	43.7	4			27	11
Tuc/Hor	45	2	6	1,32,33		
α Per	85	1,23,24	12	1	60	15
Pleiades	130	1,23,25	42	1	128	6
M35	200	26			82	16
M34	240	5			49	12
UMa	500	27	10	1		
Coma Ber	600	13			13	17
Hyades	700	28,34	41	1	50	7
M67	4000	29,18	70	1	40	8

Table 1. `BAFFLES` benchmark clusters for both calcium emission and lithium abundance. $N_{\rm Ca}$ and $N_{\rm Li}$ refer to the number of stars from each cluster with literature calcium/lithium measurements. References: (1) Mamajek & Hillenbrand (2008), (2) Bell et al. (2015), (3) Turner (2012), (4) Randich et al. (2018), (5) Meibom et al. (2011), (6) Soderblom et al. (1993), (7) Pace et al. (2012), (8) Jones et al. (1999), (9) Tobin et al. (2015), (10) King (1998), (11) Randich et al. (2001), (12) Jones et al. (1997), (13) King & Schuler (2005), (14) Mentuch et al. (2008), (15) Balachandran et al. (2011), (16) Anthony-Twarog et al. (2018), (17) Ford et al. (2001),(18) VandenBerg & Stetson (2004), (19) Shkolnik et al. (2017), (20) Pecaut & Mamajek (2016), (21) Mamajek et al. (2002), (22) de Zeeuw et al. (1999), (23) Barrado y Navascués et al. (2004), (24) Makarov (2006), (25) Duncan et al. (1991), (26) Sung & Bessell (1999), (27) King et al. (2003), (28) Brandt & Huang (2015), (29) Giampapa et al. (2006), (30) Wright et al. (2004), (31) Gray et al. (2006), (32) Jenkins et al. (2006), (33) Henry et al. (1996), (34) Gossage et al. (2018).

We used the stellar $B-V$ values if they were provided for individual stars; otherwise we used $B-V$ magnitudes from Simbad (for nearby associations with negligible reddening) or converted spectral type or T_{eff} to $B-V$. Soderblom et al. (1993) (Pleiades), Jones et al. (1997) (M34), and Jones et al. (1999) (M67) reported dereddened $(B-V)_0$, while Randich et al. (2001) (IC2602), Anthony-Twarog et al. (2018) (M35), Ford et al. (2001) (Coma Ber), and Pace et al. (2012) (Hyades) gave uncorrected $B-V$. NGC2264 lithium equivalent widths from Tobin et al. (2015) were not accompanied by $B-V$ values, so we converted spectral type to $B-V$ using the conversion in Pecaut & Mamajek (2013). For α Per (Balachandran et al. 2011), we converted T_{eff} (which had been inferred from $V-K$ color) to $B-V$ also using the conversion in Pecaut & Mamajek (2013). For β Pic (Mentuch et al. 2008; Shkolnik et al. 2017), a moving group $\lesssim$100 pc, we expect negligible reddening, and we took the observed $B-V$ colors from Simbad to be the intrinsic colors.

Close binaries present an issue since it is not always clear whether the B magnitude, V magnitude, or lithium absorption are resolved or from the combined systems. To avoid this issue, for β Pic moving group members we removed binaries from Mentuch et al. (2008): V* AZ Cap, CD-64 1208, GJ 3305, NAME AT Mic A, NAME AT Mic B, HIP 23418, LP 476-207 and binaries from Shkolnik et al. (2017): PM J01071-1935, LP 467-16, Barta 161 12, BD+17 232, CD-44 753, PM J05243-1601, GSC 06513-00291, MCC 124, TWA 22, CD-64 1208, V* AT Mic, GR* 9. We also removed stars with poorly measured values of B or V magnitudes (uncertainty $\gtrsim$0.15 mags) from Mentuch et al. (2008): HD 164249B and from Shkolnik et al. (2017): V* FK Psc, BD+30 397, EXO 0235.2-5216, 2MASS J05200029+0613036, RX J0520.5+0616, Smethells 20, CD-31 16041, TYC 6872-1011-1, TYC 7443-1102-1, BD-13 6424, UCAC4 396-055485.

For M67, we removed stars identified by Jones et al. (1999) as being less secure members, as well as potentially unresolved binaries. In many cases Li EW is given without measurement error, with the exception of Mentuch et al. (2008) and Randich et al. (2001), which did provide individual errors. For Coma Ber, we also omitted stars Ford et al. (2001) identified as non-members or spectroscopic binaries.

3. METHODS

`BAFFLES` is a Bayesian framework which finds a star's posterior age probability density function (PDF) from input of R'_{HK} or $B-V$ and Li equivalent width (Li EW). We calculate posterior PDFs according to Bayes' theorem, which for the case of calcium is given by

$$P(t|R'_{HK}) \propto P(R'_{HK}|t)P(t) \quad (1)$$

and for lithium is given by

$$P(t|LiEW, B-V) \propto P(LiEW|t, B-V)P(t) \quad (2)$$

where the three terms from left to right are the posterior, likelihood, and prior. We adopt a prior that reflects a uniform star formation rate, uniform in linear age between 0 and 13 Gyr. Although the star formation rate increases at ages older than ∼8 Gyr, this prior is a reasonable approximation for ages $<$ 5 Gyr (Snaith et al. 2015), which also corresponds to the oldest benchmark clusters we utilize. Higher-mass stars have main sequence lifetimes shorter than the full range of our prior. A stellar lifetime prior is a complicated function of $B-V$, especially since stars of a given mass evolve in color over time. Rather than commit to a particular set of isochrones, we choose to keep `BAFFLES` as empirically-driven as possible. An isochrone-based age prior can be applied to a BAFFLES posterior once generated, and we advise caution when considering an age posterior with significant probability at very large ages for higher-mass stars.

We empirically determine the likelihood functions for calcium, which depends on age, and for lithium, which depends on both age and $B-V$. For both indicators we

1. Determine the dependence of the indicator on $B-V$
2. Fit mean activity as a function of age and $B-V$
3. Fit for the astrophysical scatter PDF
4. Extend the resulting likelihood across the entire age range of the prior.

3.1. *Calcium Likelihood*

3.1.1. *The Color Dependence of R'_{HK}*

The derived quantity R'_{HK} is formulated to be independent of $B-V$ color, which is accomplished by using two polynomials in $B-V$ to convert the raw S_{HK} value into R'_{HK}. To determine the extent to which R'_{HK} is in fact independent of color we initially considered using a two-parameter linear fit to the clusters (similar to Mamajek & Hillenbrand (2008)), since the slopes seemed non-negligible. However, since our dataset included many clusters with only a handful of calcium measurements, the fit slopes were poorly determined, and the fits crossed frequently, a non-physical outcome.

As in the right panel of Figure 1, linear fits to the clusters resulted in non-monotonic changes in R'_{HK} over time, especially in the reddest and bluest regions of our $B-V$ range. Although Mamajek & Hillenbrand (2008) used linear fits for each cluster, they interpolated cluster means for solar $B-V$ ($\sim$0.65) only. For solar $B-V$, the cluster means are still monotonic, something not true for other $B-V$ values that were included in our study.

As a result, to avoid over-fitting sparse data, we adopted a constant fit for R'_{HK}, where each cluster is represented by the median value of R'_{HK}, with no $B-V$ dependence. A constant fit has the advantage of capturing the monotonic decrease in R'_{HK} while remaining the simplest fit. Mamajek & Hillenbrand (2008) advocate determining age from R'_{HK} through an age-activity-rotation relation, the effect of which is a significant $B-V$ dependence on R'_{HK} for object of similar ages (see their Figure 11), which varies by $\sim$0.15 dex across $B-V$. As there are limited R'_{HK} measurements in benchmark clusters it is currently difficult to confirm this behavior of R'_{HK} as a function of color. In fact, more direct solutions to a $B-V$ dependence of R'_{HK} would be to either redetermine the polynomial parameters or to fit directly in S_{HK}, and either would likely require a larger dataset than that presented here.

3.1.2. R'_{HK} *as a function of age*

From the fits above we have nine cluster ages and their respective mean $\log(R'_{HK})$ values, which we use to find the mean $\log(R'_{HK})$ at all ages covered by our prior. We fit $\log(R'_{HK})$ as a function of age with a second-order polynomial, constrained to be monotonically decreasing, and where each cluster in the fit is weighted by the number of stars it contains (Figure 2). Our fit is consistent with polynomial fits from previous authors. Mamajek & Hillenbrand (2008) use linear fits for finding each cluster's mean R'_{HK} as a function of $B-V$, and then fit a third-order polynomial to age, based on the values for each cluster of the linear fits at the solar $B-V$ of 0.65. The largest discrepancy between the two fits are, unsurprisingly, at ages lower than that of the youngest benchmark cluster (Upper Sco) and larger than that of the oldest (M67). Soderblom et al. (1991) experimented with several different second-order polynomials, correcting for disk heating and a uniform star formation rate.

3.1.3. *Astrophysical Scatter*

We find the width of the likelihood distribution from the scatter in each cluster, which we determine by computing the standard deviation of the R'_{HK} fit residuals for each star in the cluster. We then fit the scatter in R'_{HK} against age. In Figure 3 we observe that the scatter between 20-200 Myr is larger than the scatter for younger or older stars. This is reminiscent of Figure 1 of Gallet & Bouvier (2013), where solar-type stars spin up between $\sim$10-50 Myr as they contract when approaching the main sequence, and the dispersion in rotation rate between the fast-rotators and slow-rotators in a single cluster increases, compared to stars younger than 20 Myr or older than 200 Myr. As a result we fit a four-parameter Gaussian distribution to scatter as a function of age, as shown in Figure 3.

Since the residuals appear significantly non-Gaussian, we attempt to find an empirical fit to the distribution of residuals instead to model astrophysical scatter (Figure 4). We divide each cluster's residuals by the appropriate fit value from a Gaussian fit to standard deviation as a function of age (Figure 3). Then we empirically fit a function to the smoothed CDF of the scaled residuals, as in Figure 4, capturing the shape of the astrophysical scatter. The tails of the PDF are constrained to decrease exponentially out to 5 standard deviations and then are fixed at zero. The astrophysical scatter at each value of $\mu_L(t)$ is given by this empirical PDF, the width of which is then scaled by the inferred standard deviation (again from the fit in Figure 3).

3.1.4. *Final likelihood function*

The final likelihood function is determined by combining the PDF of astrophysical scatter (f) with the fits to mean R'_{HK} ($\mu(t)$) and standard deviation in R'_{HK} ($\sigma(t)$) at each age, as follows:

$$P(R'_{HK}|t) = f(R'_{HK}|\mu(t), \sigma(t)) \quad (3)$$

Here f is given by the residual PDF in Figure 4, $\mu(t)$ by the polynomial fit in Figure 2, and $\sigma(t)$ by the gaussian fit in Figure 3. At each age, we shift the astrophysical scatter fit, f, to be centered on $\mu(t)$, and scale it to have width $\sigma(t)$.

3.2. *Lithium Likelihood*

The overall process of finding the likelihood function for lithium is similar to the process used for calcium. Fits are made to Li EW as a function of $B-V$ for each cluster, followed by fitting Li EW as a function of age. However, there is an added complication for lithium in that the depletion of Li EW is a strong function of $B-V$, while R'_{HK} is a metric specifically designed to be independent across $B-V$ at a variety of ages. Additionally, there are significant numbers of objects at various ages where upper limits are reported for lithium equivalent width. We determine the astrophysical scatter using a numerical fit to cluster residuals. Throughout we fit to log(Li EW), since we find that the scatter in log(Li EW) is more uniform than the scatter in Li EW itself.

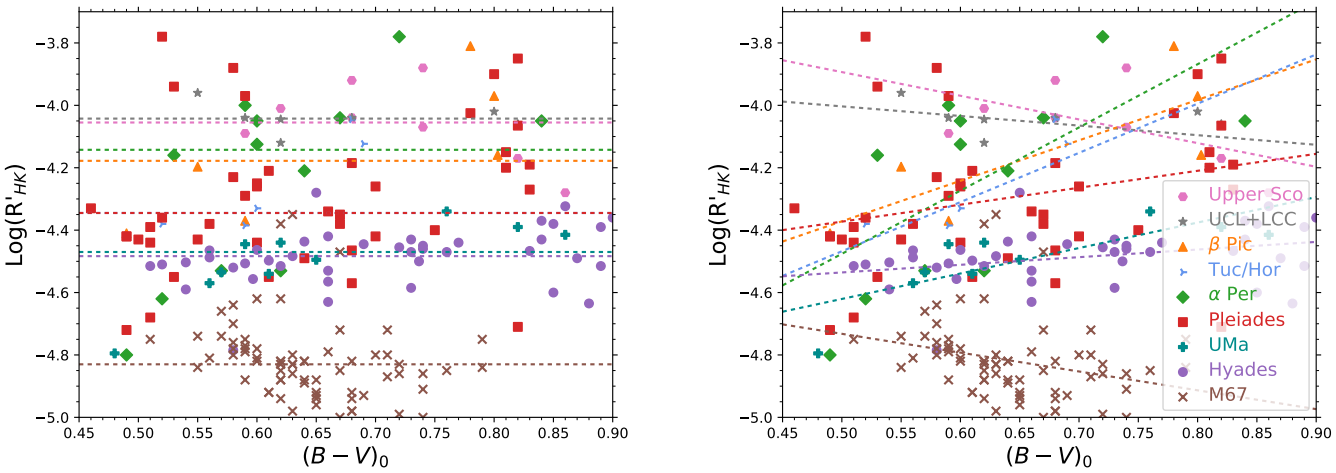

(a) One-parameter fits

(b) Two-parameter fits

Figure 1. (left) One-parameter fits with no color dependence avoid overfitting. (right) linear fits to the $B-V$ dependence of R'_{HK} for each cluster are dominated by outliers for sparse datasets, and become non-monotonic at the blue and red ends. We adopt the one-parameter fit in the final likelihood function.

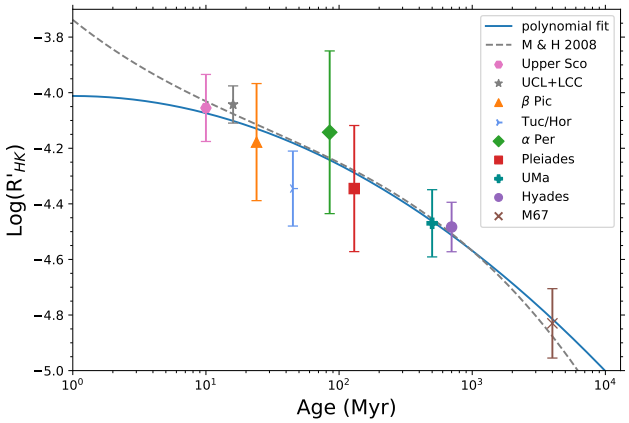

Figure 2. Fit for the mean R'_{HK} as a function of age using cluster median values. The observed variation is consistent with R'_{HK} decreasing monotonically with time. The solid blue line is our second-order polynomial fit to cluster median activity, which is mostly consistent with the overplotted third-order polynomial (gray dashed line) from Mamajek & Hillenbrand (2008), based on a nearly identical dataset.

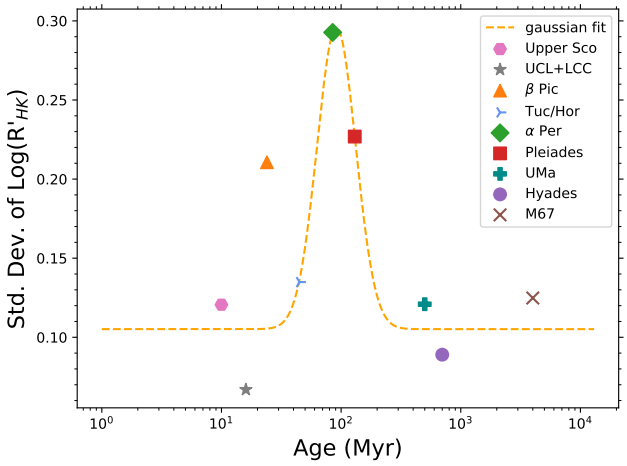

Figure 3. Standard deviation of the residuals to the fit to each calcium cluster, computed as the standard deviation of the residuals. Scatter in R'_{HK} over time appears to increase between 20 and 200 Myr, suggestive of a similar effect in the scatter of rotation rate as a function of age (Gallet & Bouvier 2013). As a result we model the scatter as a function of age as a Gaussian function in log(Age) with parameters μ=1.96, σ=0.16, amplitude=0.077, and constant offset = 0.11. There are limited numbers of young stars with R'_{HK} measurements, (8 stars each in Upper Sco and UCL+LCC, and 6 stars each in β Pic and Tuc/Hor), making our measurements of standard deviation somewhat uncertain at these ages, compared to clusters with more measurements.

3.2.1. *The Color Dependence of Li EW*

For a single cluster Li EW appears as a Gaussian or parabola as a function of $B-V$, as shown in Figure 5. The reddest stars and bluest stars in the cluster tend to have the smallest values for lithium EW while intermediate $B-V$ stars (G stars) have the largest lithium EW. This behavior is the result of two primary processes. First, redder, lower-mass stars have deeper convective envelopes so more quickly convect lithium to deeper, hotter layers of the star where it is fused, resulting in faster depletion of lithium. Meanwhile, blue stars have hotter photospheres so there are fewer lithium atoms in the ground state to absorb 6708 Å light. Stars are expected to have uniform lithium abundance (N(Li)) at formation, but this translates to a range of Li EW values

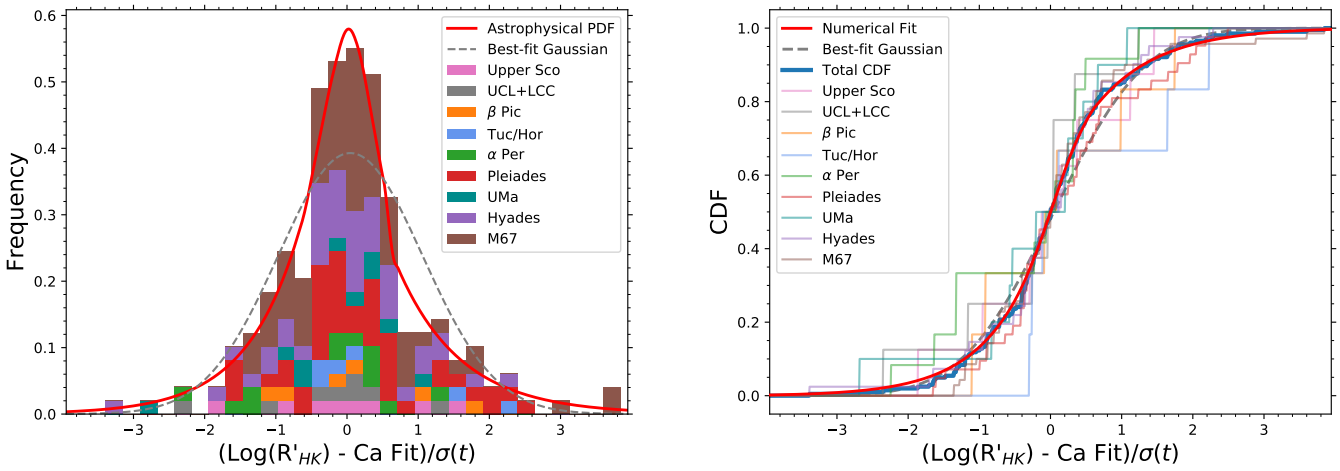

Figure 4. (left) Numerically determined astrophysical scatter PDF from cluster residuals and (right) the corresponding CDF. Residuals from each cluster are divided by the Gaussian fit to standard deviation as a function of age (Figure 3). The X-axis therefore represents the residual distance in units of standard deviations. The PDF has exponentially decreasing tails similar to the best-fit Gaussian distribution (gray dashed line) but is more sharply peaked.

as a function of color, given the different photospheric temperatures across this range. In addition to the Gaussian shape, the 'lithium dip' is observed for stars between $B-V$ of ∼0.36 and ∼0.42 (6900K and 6600K) for stars that are $\gtrsim$500 Myr, where there is a decrease in lithium abundance in this narrow range compared to stars on either side of the dip (Boesgaard & Tripicco 1986; Balachandran 1995). A suggested explanation for the "lithium dip" is that at the hot end of the dip, magnetic field strength is increasing with decreasing stellar mass, spinning down the outer layers of the star and creating turbulent mixing from internal shear between these layers and the faster-rotating core. Then moving to the cooler end of the dip corresponds to the rise of internal gravity waves, which more efficiently spin down the core, so that there is less turbulent mixing (Talon & Charbonnel 2010). Under this model, surface lithium is preferentially destroyed in the narrow region of the lithium dip, while it is preserved on either side.

In order to fit log(Li EW) as a function of $B-V$, we used a four-parameter fit: three parameters define a second-order polynomial, $\mu_L(t)$, and a fourth defines a constant astrophysical scatter, $\sigma_L(t)$, which we use temporarily to incorporate upper limits into our fit of $\mu_L(t)$. To fit these parameters we assumed a Gaussian likelihood, which for lithium detections takes the form:

$$P(log(LiEW)|t, B-V) = \frac{1}{\sqrt{2\pi}\sigma_L(t)} e^{\frac{(log(LiEW)-\mu_L(t))^2}{2\sigma_L(t)^2}} \quad (4)$$

For lithium upper limits (LiUL) we represent the likelihood as the integral of the Gaussian function from -∞ to the upper limit (where $\mu_L(t)$, $\sigma_L(t)$ and LiUL are all log quantities):

$$P(LiUL|t, B-V) = \int_{-\infty}^{LiUL} \frac{1}{\sqrt{2\pi}\sigma_L(t)} e^{\frac{(x-\mu_L(t))^2}{2\sigma_L(t)^2}} dx \quad (5)$$

The lithium dip is clear in the ∼700 Myr Hyades dataset, so we fit an inverted Gaussian to the dip ($0.39 < B-V < 0.52$), and a second-order polynomial the the stars outside the dip. There is no clear evidence for a lithium dip at younger ages in M34 (∼200 Myr), and by ∼4 Gyr, stars have evolved off the main sequence leaving no stars bluer than $B-V \approx 0.5$ in M67.

3.2.2. *Li EW as a function of age*

Unlike R'_{HK}, Li EW varies substantially across both age and $B-V$. As a result, the decline in lithium equivalent width as a function of age must be fit across multiple slices of $B-V$. The polynomials fit to each cluster define μ_L as a function of $B-V$ at the age for each individual cluster. We examine 64 $B-V$ slices uniformly spaced between $B-V$ of 0.35 and 1.9. At each slice, then, we have 10 values of μ_L corresponding to our 10 cluster datasets to which we added two additional points from primordial Li EW and Blue Lithium Depletion Boundary (described below), and from these we determine the 64 fits to μ_L as a function of age.

To help constrain the young end of the fits of Li EW and age, we approximate primordial Li EW using the MIST model isochrones (Choi et al. 2016) in conjunction with our NGC2264 fit. In particular, we seek to extend the fit to this ∼5 Myr cluster to the first age point in

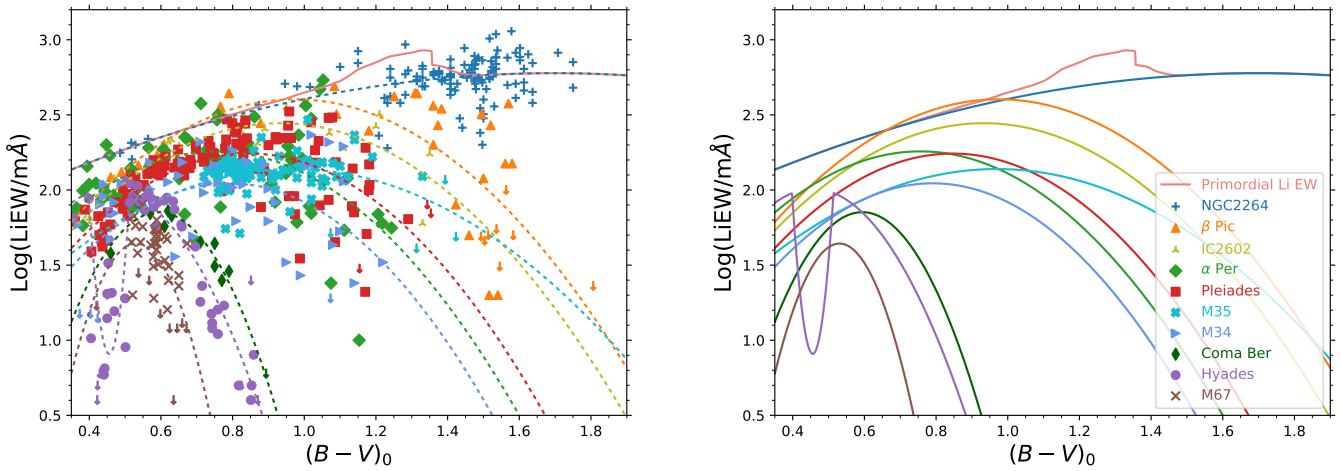

(a) Full lithium dataset and fits to each cluster

(b) Fits only

Figure 5. Lithium equivalent width measurements for our full dataset, and final fits to each cluster. Overall, second-order polynomials provide good fits to each cluster, with the addition of the lithium dip for the Hyades. Primordial Li EW is estimated from MIST isochrones in conjunction with our fit to NGC2264.

our grid, 1 Myr. At every $B-V$ value we determine the corresponding effective temperature using the conversions from Pecaut & Mamajek (2013), then we find the Li abundance, N(Li), and initial stellar mass at 5 Myr from the MIST isochrones. We then find the Li abundance from the same initial mass star using the 1 Myr isochrones. T_{eff} and Li abundance are converted to Li equivalent width using the curve of growth in Soderblom et al. (1993) for $T_{eff} > 4000K$ and Zapatero Osorio et al. (2002) for $T_{eff} \leq 4000K$. The difference in Li EW between 1 Myr and 5 Myr is added to the fit to NGC2264 to determine the primordial Li EW at every $B-V$ value (Figure 5). The MIST isochrone correction between 1 and 5 Myr is only significant between $0.8 \lesssim B-V \lesssim 1.4$, and is negligible elsewhere.

We define the Blue Lithium Depletion Boundary (BLDB) as the $B-V$ color for which stars redder than this boundary have no detectable lithium absorption, which we use to help constrain the older and redder range of fits to Li EW against age. Since the redder stars have deeper convective envelopes they burn lithium faster than the bluer stars in the cluster. As a result the nested polynomials of Figure 5 generally get narrower and move blueward over time, and thus the BLDB point moves blueward with increasing age. The BLDB is distinct from the classical lithium depletion boundary (LDB) which moves redder over time as a cluster's high-mass brown dwarfs deplete their lithium, while at the same time all brown dwarfs and pre-main sequence M stars evolve to redder colors as they cool. We have defined the BLDB in order to add an additional data point to our fits for $B-V > 0.7$, most important

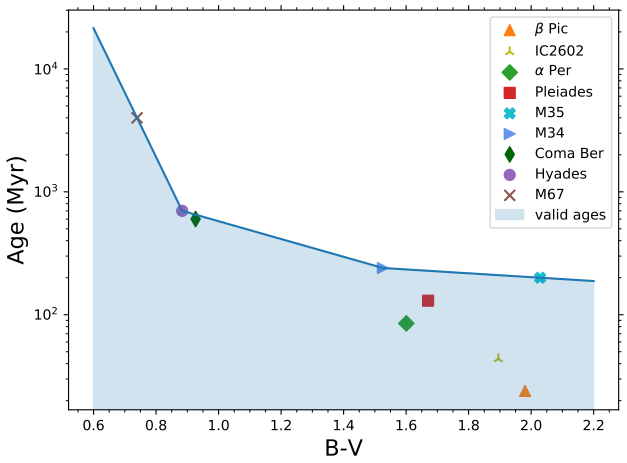

Figure 6. We introduce the concept of the Blue Lithium Depletion Boundary (BLDB), which represents the age at each $B-V$ slice where lithium equivalent width drops below 3.2 mA, to constrain the lithium abundance at the oldest ages. Each point represents the $B-V$ magnitude where our polynomial fit to each cluster (log(Li EW) vs $B-V$) goes below log(Li EW) = 0.5 or 3.2 mÅ, which we adopt as the lowest detectable equivalent width of the lithium line. Redward of the BLDB point, we expect all stars in the cluster have no detectable lithium 6708 Å absorption. We adopt a piecewise linear fit such that all clusters are at or below the fit.

for constraining the ages of stars with $B-V > 1.4$ for which there are fewer literature measurements, especially at older ages. For each $B-V$ slice redward of 0.7, the fit to BLDB points gives an approximation of

maximum age associated with log(Li EW) = 0.5, or Li EW = 3.2 mÅ (Figure 6).

For each value of $B-V$ we use the mean value of log(Li EW), μ_L, from each cluster in addition to the primordial lithium point and BLDB point to fit the intermediate ages between the cluster ages and complete our grids. Unlike calcium, where the fits to individual clusters were independent of $B-V$, for lithium there is a strong $B-V$ dependence, and for redder regions, the fit to the mean equivalent width reaches unphysically small values. When cluster means drop below ∼3mÅ (0.5 on the log scale), we don't expect any detections, and clusters with μ_L below this value are not included in the fitting process.

As in Figure 7, we fit a 2-4 segment piecewise function to the cluster means, primordial Li EW, and BLDB point. The first segment is always between the Primordial Li EW value and NGC2264 and the fit is constrained to decrease monotonically with age. The locations of the segment breaks (except for the first break at NGC2264) were free parameters. Weights for the cluster means were determined based on the relative proportion of stars the cluster had at a given $B-V$ slice in relation to the total number of stars. The BLDB point is given uncertainty about 0.15 dex compared to 1 dex for clusters in not well constrained regions. Although for some $B-V$ ranges different functional forms were good fits to the decrease in lithium over time, only the piecewise function was flexible enough to capture the shape more generally.

3.2.3. *Astrophysical Scatter*

With our grid of 64 $B-V$ slices and 1000 age slices for mean equivalent width of lithium, μ_L, we next determine the PDF of the astrophysical scatter by fitting a probability density function to the residuals for each star in log space (Figure 8). Residuals are with respect to the value of μ_L found from the polynomial fit to each specific cluster, and upper limits are not considered in this step. As with calcium, we smooth the CDF of the residuals with Savitzky–Golay filters and take the derivative to convert to a PDF. Then we fit exponential functions to the two tails, which we connect with the smoothed PDF. Unlike calcium, we find no evidence for the width of this PDF changing with age, and adopt this numerical PDF for all ages.

3.2.4. *Final likelihood function*

We fit for mean Li EW on a dense grid covering $B-V$ from 0.35 to 1.9 and age from 1-13,000 Myr. We calculate this grid of 64,000 elements (64 $B-V$ x 1000 age, logarithmically spaced in age) by interpolating between the clusters in Table 1, and store it for future use. Then for any input of $B-V$ and Li EW, we use the grid to calculate the likelihood function for the given $B-V$ value over the range of possible ages.

We determine the probability of observing a star with $B-V$ $bmv \pm bmv_{err}$ and Li EW $li \pm li_{err}$ using the astrophysical scatter PDF and the fit to mean Li EW. At a single $B-V$ slice, we represent measurement uncertainty as a gaussian centered on the measured value of Li EW, with standard deviation equal to the measurement error. If no measurement uncertainty is given we use a default error of 15mÅ, found by Soderblom et al. (1993). The likelihood for this $B-V$ slice is then the product of the astrophysical scatter PDF and the measurement gaussian. As the measurement gaussian is in linear space, to perform the multiplication we first convert the astrophysical scatter given in $\log(LiEW)$ to linear space, and shift it to be centered on the mean Li EW for that $B-V$ slice, $\mu_L(t)$:

$$PDF_{linear}(LiEW|t) = \frac{PDF_{log}(log(LiEW) - \mu_L(t))}{LiEW} \quad (6)$$

Lastly to incorporate error in $B-V$, we repeat this process for 15 sampled $B-V$ values around $B-V$=bmv and sum the results, weighted by a gaussian PDF ($\mu = bmv$, $\sigma = bmv_{err}$). If no $B-V$ uncertainty is given we use a default value 0.01 mags.

If the measurement is an upper limit, we instead integrate the astrophysical scatter PDF from $-\infty$ to the upper limit at each age. Thus, upper limits result in a plateau of probability at old ages, with a rapid drop-off toward younger ages.

4. VALIDATION

4.1. *Self-consistency of age posteriors*

To test `BAFFLES` for self-consistency, we compare the posteriors for stars in moving groups and associations to the known ages of the groups, which we show for some clusters in Figure 9. We compute posteriors for each star in a cluster and then multiply the posteriors together, assuming the age determination for each star is independent, to produce a probability density function for the age of the cluster as a whole. As an additional test, we repeat the process, but beforehand remove the target cluster from the input clusters used to fit mean R'_{HK} vs Age (though leave the cluster in for scatter vs age fits and computing the PDF of astrophysical scatter).

`BAFFLES` ages determined from calcium posterior products matched well with isochronal ages (Figure 9). The accepted isochronal ages determined from more robust techniques like main-sequence turnoff fell within

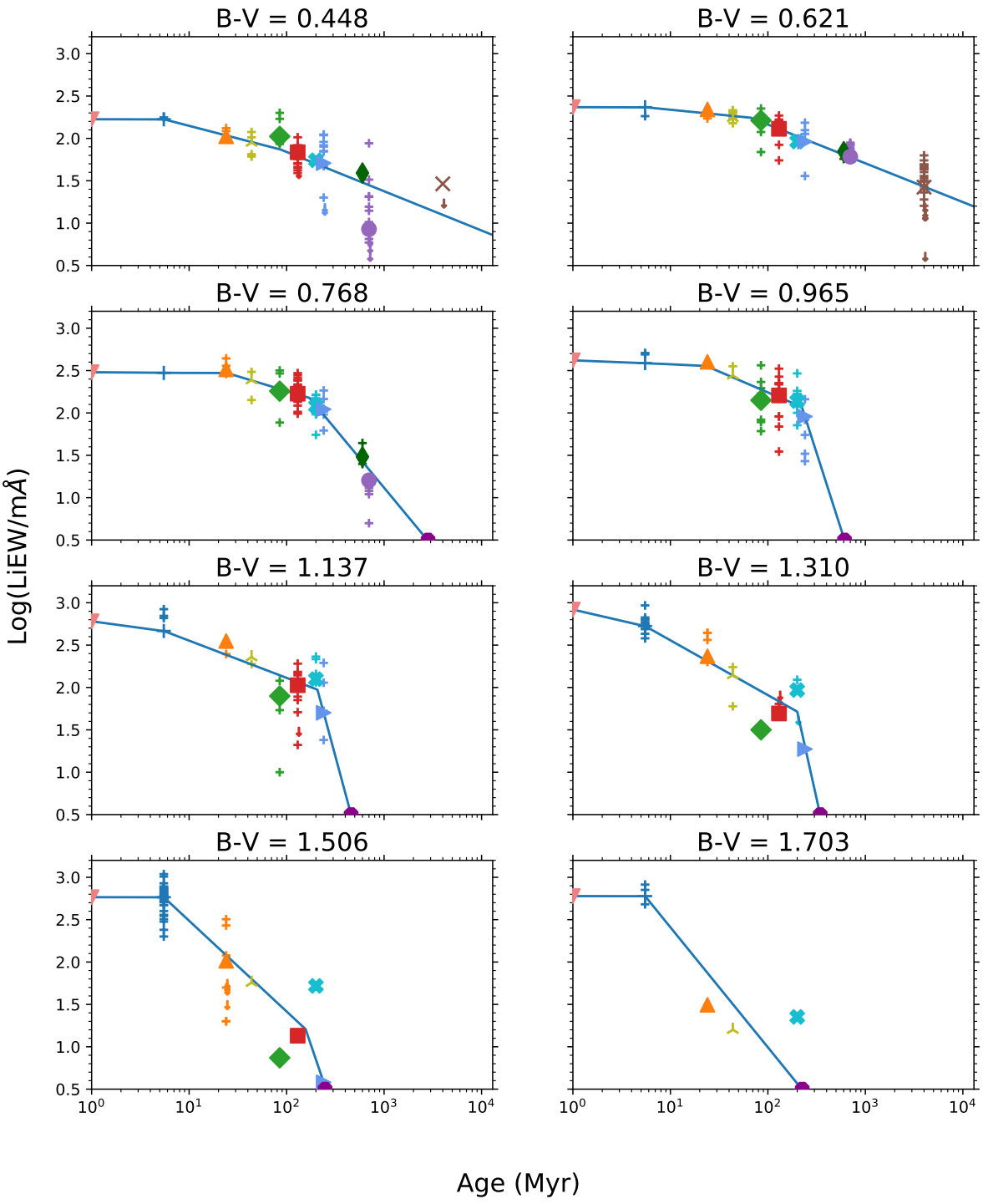

Figure 7. Examples of Li EW fits as a function of age, for eight out of 64 $B-V$ slices between 0.35 and 1.9 mags. Stars from each cluster within 0.05 mags of the $B-V$ slice are shown as small crosses if detections or downward-facing arrows if upper limits. Cluster symbols are as in Figure 5, with an additional magenta BLDB point at log(Li EW)=0.5. The cluster means were fit with a flexible piecewise-linear function fixed to the primordial lithium point and NGC2264. Cluster means were weighted to give those with the most stars at each $B-V$ slice the most weight.

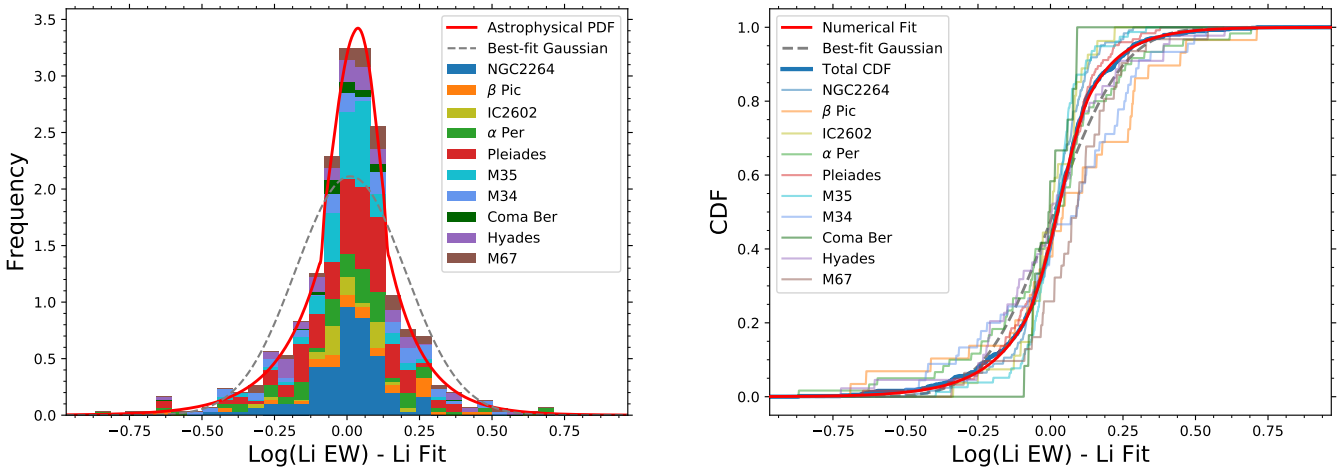

Figure 8. (left) Numerically determined astrophysical scatter PDF to the residuals from our fits to each cluster and (right) the corresponding CDF. Similarly to calcium, the numerical PDF has exponentially decreasing tails similar to a gaussian distribution but is significantly more peaked.

our 68% confidence intervals (from posteriors without removal of any benchmark clusters) in four out of nine cluster, within our 95% confidence intervals in six out of nine cluster, and within the 98.5, 99.5, and 99.0% confidence intervals for β Pic, Tuc/Hor, and Hyades. Both β Pic and Tuc/Hor have only six stars so the age is not well determined. The reason for the offset in the Hyades is less evident, though we note that since the cluster age posterior is the product of multiple PDFs, a single non-member, incorrect measurement, or other outlier can significantly shift the final posterior. This result suggests that the median ages determined by BAFFLES from its input clusters are self-consistent, and that the confidence intervals are reasonable.

A similar posterior product check with lithium clusters found agreement with isochronal values (as seen in Figure 10). NGC2264, β Pic, IC2602, Pleiades, M35, and M34 agree with isochronal ages to within 68% CI, and α Per and Coma Ber agree within 95% CI. Hyades and M67 have isochronal ages that are younger than the median BAFFLES ages, and are within the 99.8 and 98.6% confidence intervals, respectively. The offset in the Hyades is likely due to how the lithium dip is handled, with an older age assigned to dip stars compared to the other stars in the cluster. Computing the age of the Hyades with only stars of $B-V > 0.55$ (excluding all dip stars), the isochronal age falls within our 75% confidence interval. As with calcium, a product of posteriors is very sensitive to each individual posterior, so that a single non-member, or errors in color or lithium abundance, can move the product significantly from the age of the group as a whole. We conclude that the age posteriors generated by BAFFLES are consistent with the ages of our benchmark clusters.

4.2. *Moving Groups*

We further examine the accuracy of BAFFLES age posteriors by considering the ages derived for multiple stars in moving groups not included in our set of benchmark clusters. As before, we compute age PDFs for each star in the moving group and then multiply the PDFs together to find an age for the group as a whole, which we compare to isochronal ages from Bell et al. (2015) (Figure 11).

Lithium equivalent widths for AB Dor and Tuc/Hor are from Mentuch et al. (2008), and $B-V$ magnitudes are from the Simbad online services. From AB Dor we removed the binaries HD 13482A, HD 13482B, HD 17332B, HD 217379N, HD 217379S and also stars with large $B-V$ uncertainties (error $\gtrsim$0.15 mags): BD+21 418B. From Tuc/Hor we removed the binaries:V* AF Hor, V* BS Ind, HIP 116748N, HIP 116749S, TYC 7065-0879N, TYC 7065-0879S as well as stars with error $\gtrsim$0.15 mags: EXO 0235.2-5216, CD-58 553, Smethells 86, V* CT Tuc, Smethells 165, Smethells 173.

We derive ages for AB Dor: 140^{+34}_{-27} Myr, and Tuc/Hor: 41^{+10}_{-8} Myr, as in Figure 11. These ages largely agree with isochronal ages – AB Dor 149^{+51}_{-19}, Tuc/Hor 45^{+4}_{-4} Myr – from Bell et al. (2015). We caution against using the ages we derive for these moving groups, however, since our posterior products can be significantly biased by a single star with incorrect values (either lithium abundance, B or V), or with an incorrect membership determination.

5. ANALYSIS

5.1. *Notable Stars: TW PsA, HR 2562, and HD 206893*

We show examples of ages derived using BAFFLES for three field stars associated with substellar companions: the brown dwarf hosts HR 2562 and HD 206893, and the stellar companion to the exoplanet host Fomalhaut, TW PsA. Age sets the formation timescale for these substellar companions, and in the case of the brown dwarfs, the model mass derived for these objects depends directly on the assumed age.

TW PsA is a stellar companion to the A3V star Fomalhaut with a bright debris disk and planetary companion. The system's age has been estimated by Mamajek (2012) to be 440 ± 40 Myr by combining independent age estimates from isochrones, rotation rate, X-ray luminosity, and lithium abundance. From lithium alone, Mamajek (2012) estimates an age of 360 ± 140 Myr by comparing the Li EW of TW PsA, with values $B-V$=1.1 (Simbad) and Li EW=33±2 (Barrado y Navascués et al. 1997), to the Li EW in the clusters Pleiades, M34, UMa, Hyades. Using these same values of $B-V$ and Li EW as input to BAFFLES, we report an age of 305 Myr with a 68% confidence interval between 257 Myr - 371 (third panel of Fig. 12), consistent with the Mamajek (2012) lithium age, but a factor of ∼1.4 too young for the final adopted age. However at $B-V$=1.1, we are limited by our cluster samples which have lithium detections up to the age of M34 (240 Myr), and non-detections at the age of Coma Ber (600 Myr), but no information in between. Thus interpolations to older ages at this $B-V$ are difficult with our current dataset.

We also combine our age PDF with that for the A star Fomalhaut from Nielsen et al. (2019), 750^{+170}_{-190} Myr, with our PDF (middle-right plot of Fig. 12), to get a final age for the system, 300^{+40}_{-30} Myr. Since the distribution from BAFFLES is significantly narrower than that from Nielsen et al. (2019), the product age changes little, yet this serves as an example of how an age posterior allows

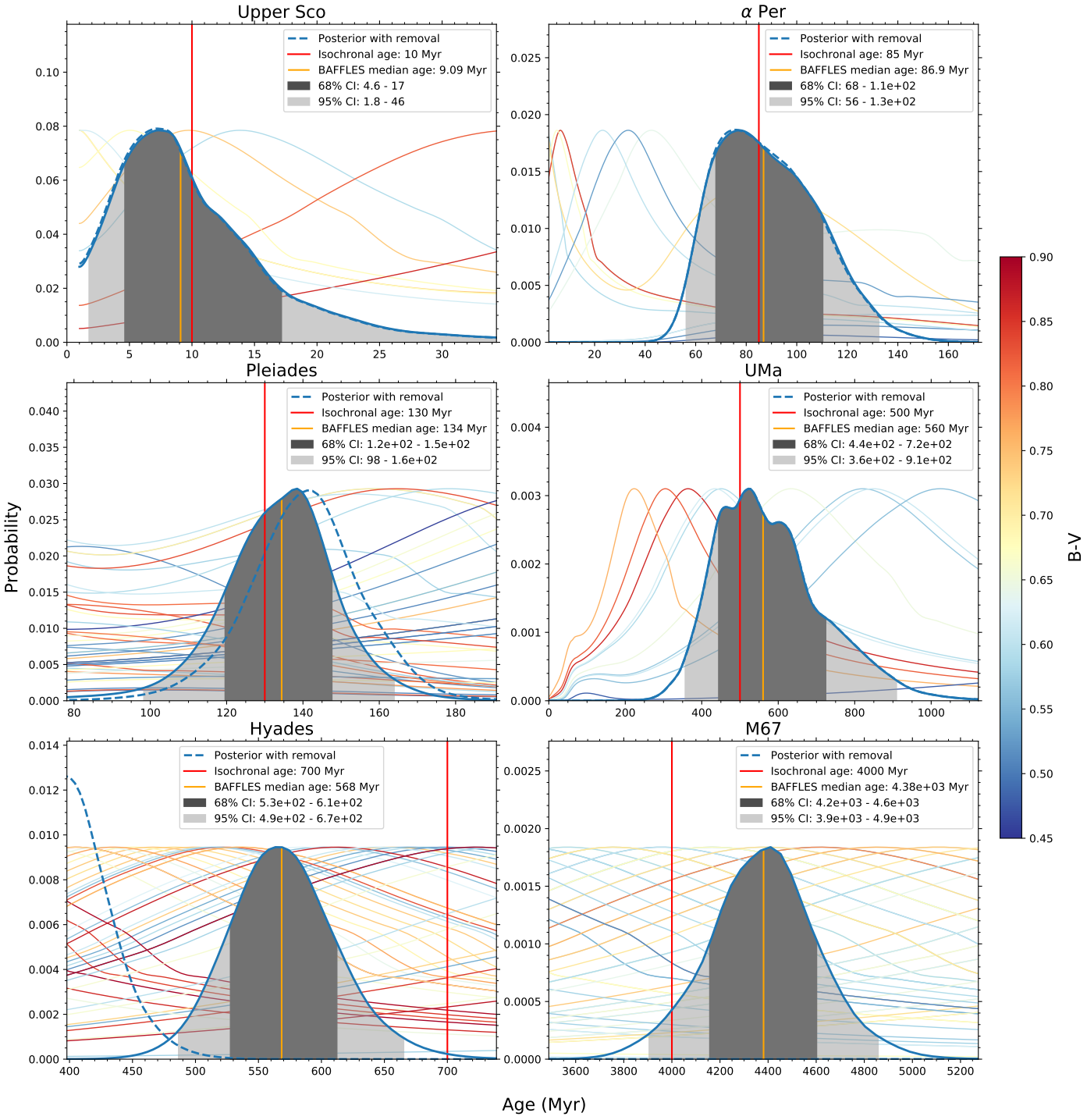

Figure 9. We test the validity of our calcium age posteriors by considering the product of PDFs from every star in one of our benchmark clusters, which should represent the PDF of the cluster age. We calculate the age posteriors for each star in the cluster (shown color-coded by $B-V$ and scaled to common height in the background), and finally multiply the age posteriors together to get the posterior product. The blue dashed line is the posterior product produced if we first omit the cluster from those used to calibrate `BAFFLES`. "Isochronal Age" represents the more robustly determined ages from Table 1 that we use as the ages of our benchmark clusters. The mostly 1-2 σ agreement suggests the median age and uncertainties we find with `BAFFLES` are consistent.

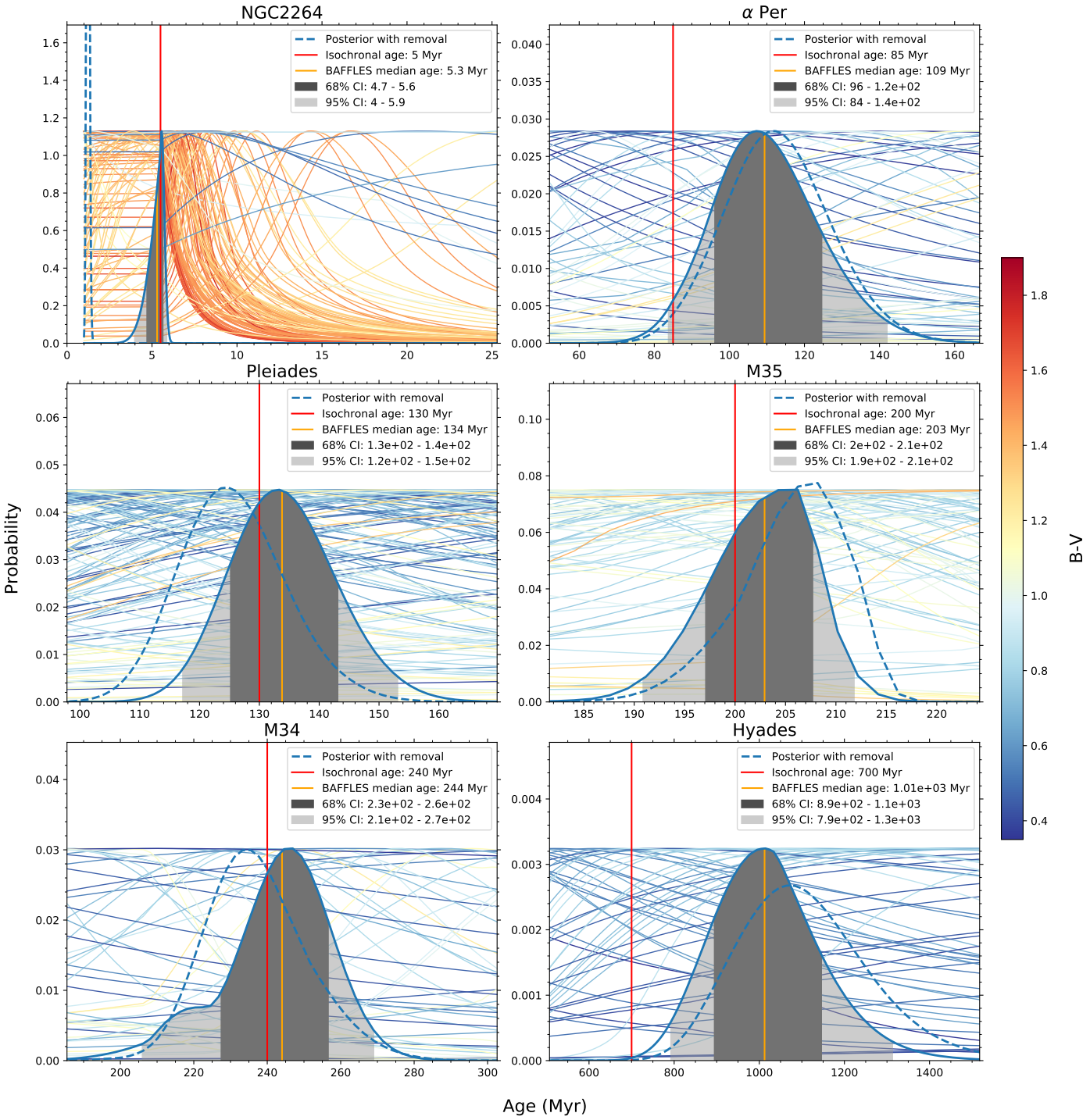

Figure 10. Following Figure 9, we test the validity of our lithium posteriors. Our ages are consistent with isochronal ages to within 95% confidence intervals for all clusters except Hyades and M67, which have isochronal ages that are younger than our median ages and are within the 99.8 and 98.6% confidence intervals. If we recompute the Hyades age with only stars of $B-V > 0.55$, to exclude the 'lithium dip', the isochronal age of 700 Myr falls within our 75% confidence interval, which suggests the Hyades age discrepancy is due to how we handle the dip.

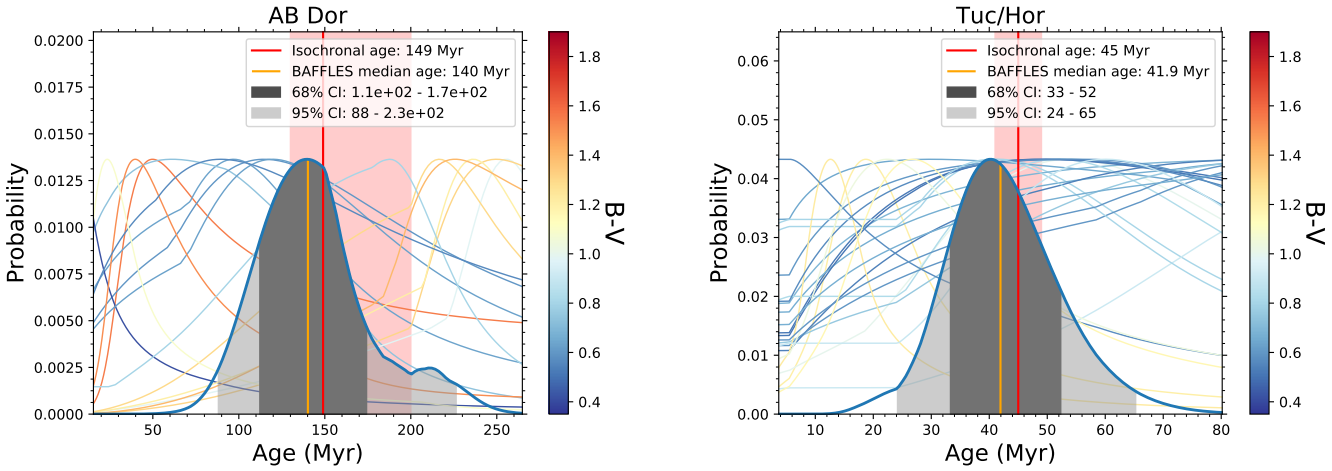

Figure 11. We compute age posteriors for AB Dor and Tuc/Hor from the product of the posteriors of stars in each cluster. Our computed ages largely agree with isochronal values, suggesting that our lithium-derived posteriors are generally accurate. Data for AB Dor and Tuc/Hor is from Mentuch et al. (2008) and isochronal ages are from Bell et al. (2015).

ages from `BAFFLES` to be robustly combined with ages from other sources.

HR 2562 is an F5V star around which a brown dwarf companion was discovered with the Gemini Planet Imager in 2016 (Konopacky et al. 2016). Asiain et al. (1999) estimated the age to be 300 ± 120 Myr based on space motions and evolutionary model-derived ages. Casagrande et al. (2011), using Strömgren photometry and isochrones, derive a Bayesian age of 0.9-1.6 Gyr (68% confidence interval). From calcium alone with $\log(R'_{HK}) = -4.551$ (Gray et al. 2006), we report an age of 1200 Myr (68%CI: 700 - 3000 Myr). From lithium alone, using Li EW = 21 ± 5 (Mesa et al. 2018) and $B - V$=0.45 ± .02 (Simbad), we find an age of 4.4 Gyr (68%CI: 1.8 - 9.1 Gyr). We note that HR 2562 is in the very center of the lithium dip, and so our lithium age is likely overestimated due to how the piecewise fits of Li EW vs. age handle the dip. Combining these posteriors, our final age is 1400 Myr, with a 68% confidence interval between 870 Myr - 2900 Myr, consistent with the age range 300-900 Myr adopted by Konopacky et al. (2016).

HD 206893 is an F5V star with a brown dwarf companion inside its debris disk (Milli et al. 2017). Pace (2013) derives its age to be 860 ± 710 Myr from chromospheric activity. On the other hand David & Hillenbrand (2015) derive an age of 2.1 Gyr with 68% CI between 1.2 - 4.7 Gyr using a Strömgren photometry fit to stellar atmosphere models, though given the long main-sequence lifetime of early F stars, this method is not particularly sensitive to the differences between young and intermediate ages (e.g. Nielsen et al. (2013)). Milli et al. (2017) adopts an age range between 200 - 2100 Myr. Using a value of $\log(R'_{HK}) = -4.466$ (Gray et al. 2006), from calcium emission alone we derive a median age of 710 Myr (68%CI: 400 - 2000 Myr). From lithium absorption with Li EW = 28.5 ± 7 mÅ (Delorme et al. 2017) and $B - V$=0.44 ± 0.02 (Høg et al. 2000), we report an age of 3.0 Gyr (68%CI: 1.1 - 7.6 Gyr), though like HR 2562, HD 206893 is also in the center of the lithium dip, with a likely overestimated age. Our final age after combining these two posteriors is 780 Myr, with a 68% confidence interval between 490 Myr - 1700 Myr, consistent with literature ages.

We find that `BAFFLES` age posteriors for these field stars are consistent with literature ages. Both HR 2562 and HD 206893 are within the lithium dip where our fits to Li EW vs age level off at older ages (Figure 7). As a result the ages derived from lithium alone are not well constrained and are likely overestimated, and our final ages from combining calcium and lithium are primarily determined by the calcium posterior. In general, however, lithium-based ages are often more constraining than calcium-based ones, given that the astrophysical scatter in R'_{HK} is a more significant fraction of the total range of R'_{HK}. Nevertheless, the combination of these two methods tends to increase the precision on the final age posterior.

5.2. *Comparison to previous methods*

The `BAFFLES` median ages are systematically older than those derived from Mamajek & Hillenbrand (2008) R'_{HK} polynomial despite relying on the same clusters and very similar fits to the clusters (Figure 2). In the Pleiades and Hyades, for example, the median age we derive for each star with `BAFFLES` is older than the age given by the polynomial fit of Mamajek & Hillen-

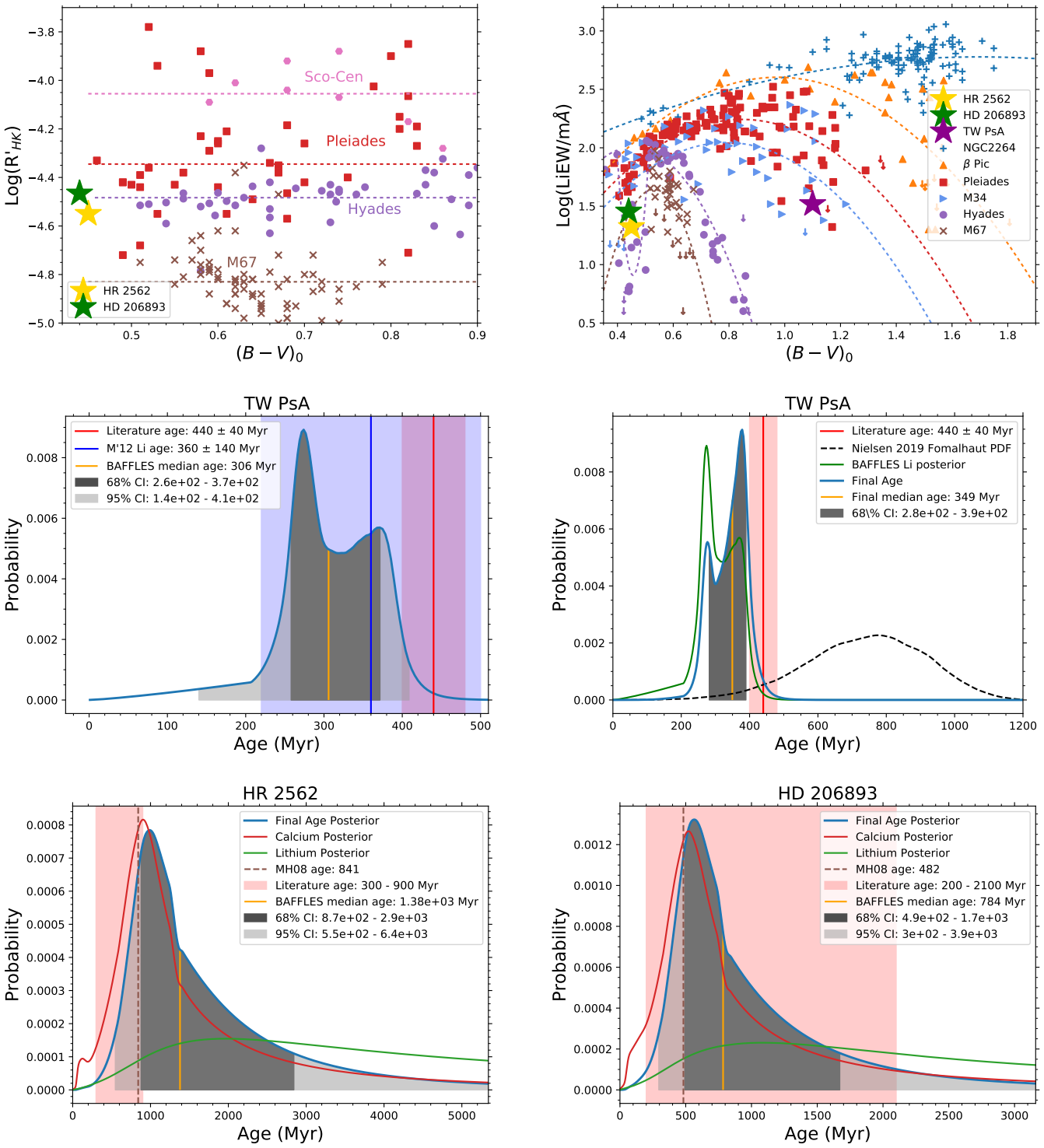

Figure 12. `BAFFLES` age posteriors for three notable field stars from calcium R'_{HK} and lithium equivalent width. The top panel shows the measurements of $B-V$, R'_{HK}, and Li EW of the stars in comparison with a subset of our benchmark clusters. We then compare the age posterior computed using `BAFFLES` to ages from the R'_{HK} polynomial in Mamajek & Hillenbrand (2008) ("MH08 age", though we again note that Mamajek & Hillenbrand 2008 advocate a modified R'_{HK} relation incorporating additional correlations as well) and literature ages from Mamajek (2012); Konopacky et al. (2016); Milli et al. (2017) for TW PsA, HR 2562, and HD 206893, respectively. For HR 2562 and HD 206893, age posteriors for calcium and lithium are multiplied together to find a final age, although the lithium posteriors are not well constrained due to a leveling off of our fits at $B-V$ ~0.45 at older ages (Figure 7). The middle right plot demonstrates combining a posterior from `BAFFLES` with the PDF from a different source, in this case the age PDF for Fomalhaut derived by Nielsen et al. (2019).

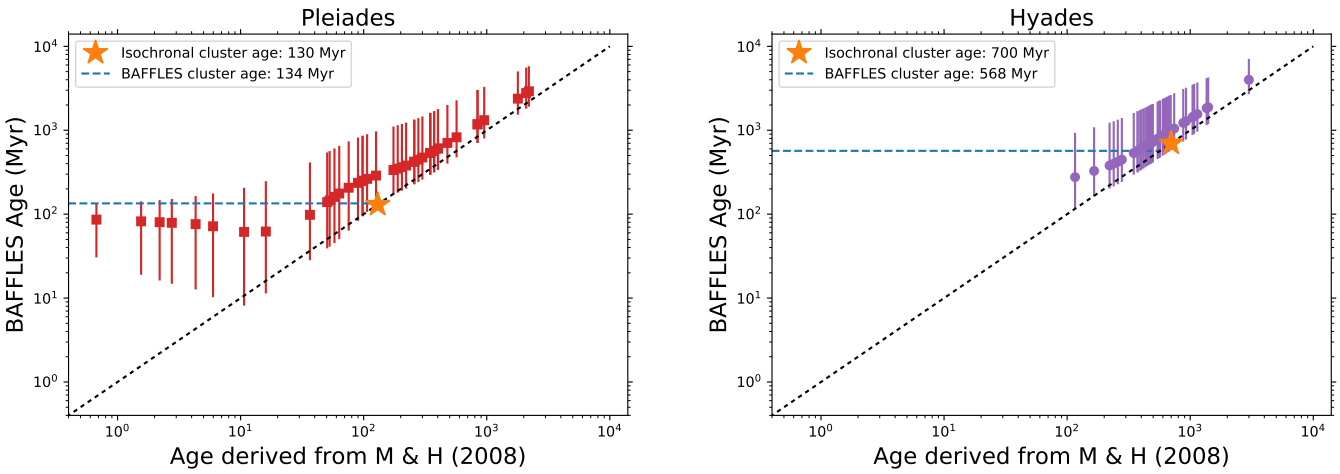

Figure 13. Comparison of `BAFFLES` calcium age posteriors to stellar ages derived from the polynomial fit (Eq. 3) from Mamajek & Hillenbrand (2008). Error-bars indicate the 68% confidence interval from `BAFFLES`. As expected from a prior uniform in linear age, the median of the posterior for each individual star is systematically older than the age determined by the Mamajek & Hillenbrand (2008) polynomial fit. Additionally, the larger astrophysical scatter at ∼100 Myr results in similar ages for the most active stars. Nevertheless, the product of these individual posteriors (Figure 9) shows that taken together, these posteriors converge on the correct age for the cluster as a whole.

brand (2008) (Figure 13). Our likelihood function is roughly gaussian in log(age), with the median moving to more negative values of R'_{HK} approximately uniformly in log(age), but a uniform prior systematically shifts the median of the posterior to older ages by de-weighting younger ages and adding extra weight to older ages, since young stars are intrinsically less common than older stars. As a result, omitting a prior of uniform star formation may systematically find ages that are too young.

5.3. `BAFFLES` *ages for young, nearby stars*

We use our method, `BAFFLES`, for a sample of 2630 nearby stars that appear in recent compilations of lithium measurements, R'_{HK} measurements, or direct imaging surveys. In Table 2 we derive the ages of stars from the analysis of two direct imaging planet surveys by Nielsen & Close (2010), from the SEEDS High-contrast Imaging Survey of Exoplanets and Disks (Brandt et al. 2014a), from the compilation of R'_{HK} values by Boro Saikia et al. (2018), and from the lithium measurements in the spectroscopic survey of Guillout et al. (2009). Boro Saikia et al. (2018) compiled R'_{HK} values from a number of previous literature surveys, including Arriagada (2011); Wright et al. (2004); Isaacson & Fischer (2010); Henry et al. (1996); Gray et al. (2006); Hall et al. (2009); Lovis et al. (2011); Bonfils et al. (2013); Duncan et al. (1991); Baliunas & Vaughan (1985). Guillout et al. (2009) acquired lithium and $H\alpha$ measurements of several hundred field stars.

We compute age posteriors for each unique star from R'_{HK} and Li EW separately, and when both are available, we multiply these posteriors to determine a final age. For stars with multiple entries, we first compute the mean values of $B-V$, R'_{HK} and Li EW over all measurements, then use these means to find the age posteriors.

Table 2. BAFFLES ages for nearby stars

Name	RA	Dec	Sp. Type	$B-V$	$\log R'_{HK}$	Li EW	Ref.	R'_{HK} Age at Posterior CDF Value (Myr)					Li EW Age at Posterior CDF Value (Myr)					Final Age at Posterior CDF Value (Myr)				
	h m s	h m s		mags		(mÅ)		2.5%	16%	**50%**	84%	97.5%	2.5%	16%	**50%**	84%	97.5%	2.5%	16%	**50%**	84%	97.5%
BD+35 5152	00 00 35.97	+36 40 7.56	G0	0.66		104	4						76	195	**345**	785	3050	76	195	**345**	785	3050
HD 224783	00 00 38.12	−66 40 59.43	G2IV/V	0.55	−4.78		3	1410	2650	**3940**	7040	11500						1410	2650	**3940**	7040	11500
HD 224789	00 00 40.32	−69 40 33.48	K1V	0.86	−4.53		3	261	640	**1080**	2830	8160						261	640	**1080**	2830	8160
CCDM J00014+3937AB	00 01 23.66	+39 36 38.56	K0	0.82		24	4						378	630	**1630**	3390	5320	378	630	**1630**	3390	5320
* 85 Peg	00 02 10.34	+27 04 54.48	G5VbFe-2	0.67	−4.84		3	1950	3570	**5190**	8310	12000						1950	3570	**5190**	8310	12000
HD 224983	00 02 21.54	+11 00 22.46	K0V	0.89	−4.99		3	3890	6840	**9450**	11600	12700						3890	6840	**9450**	11600	12700
HD 225118	00 03 41.48	−28 23 46.30	G8.5V	0.77	−4.49		3	186	487	**844**	2320	6800						186	487	**844**	2320	6800
HD 225239	00 04 53.72	+34 39 34.80	G3	0.63	−4.89		3	2520	4550	**6480**	9380	12300						2520	4550	**6480**	9380	12300
HD 225261	00 04 56.32	+23 16 10.66	G9V	0.76	−4.95		3	3300	5860	**8180**	10600	12600						3300	5860	**8180**	10600	12600
HD 225299	00 04 58.72	−70 12 44.79	G5V	0.71	−4.85		3	2010	3670	**5310**	8420	12000						2010	3670	**5310**	8420	12000
HD 5	00 05 10.18	+02 23 49.96	G2/3V	0.62	−4.70		3	859	1690	**2600**	5350	10600						859	1690	**2600**	5350	10600
HD 225297	00 05 2.63	−36 00 54.43	G0V	0.54	−4.77		3	1340	2520	**3760**	6830	11400						1340	2520	**3760**	6830	11400
HD 39	00 05 29.05	+34 06 20.56	F8	0.51	−4.78		3	1420	2660	**3950**	7050	11500						1420	2660	**3950**	7050	11500
HD 105	00 05 52.54	−41 45 11.05	G0V	0.59	−4.33		3	58	172	**338**	1120	3330						58	172	**338**	1120	3330
HD 23	00 05 7.50	−52 09 6.26	G0V	0.58	−4.76		3	1230	2330	**3500**	6530	11200						1230	2330	**3500**	6530	11200
HD 24	00 05 9.80	−62 50 42.79	G0V	0.59	−4.38		3	85	223	**414**	1320	4020						85	223	**414**	1320	4020
HD 123	00 06 15.81	+58 26 12.22	G3V+G8V	0.68	−4.56		3	325	755	**1250**	3160	8610						325	755	**1250**	3160	8610
HD 142	00 06 19.18	−49 04 30.68	F7V	0.52	−4.77		3	1320	2490	**3720**	6790	11400						1320	2490	**3720**	6790	11400
HD 166	00 06 36.78	+29 01 17.41	G8	0.75	−4.36		3	72	197	**372**	1210	3680						72	197	**372**	1210	3680
HD 232102	00 06 37.38	+55 27 21.72	K0	0.92		4	4						366	501	**755**	1020	1230	366	501	**755**	1020	1230
HD 283	00 07 32.54	−23 49 7.40	G9.5V	0.80	−4.98		3	3710	6550	**9070**	11300	12700						3710	6550	**9070**	11300	12700
HD 299	00 07 52.09	+55 34 37.35	G0	0.60		67	4						331	931	**2830**	7770	12000	331	931	**2830**	7770	12000
HD 361	00 08 16.36	−14 49 28.17	G1V	0.62	−4.80		3	1560	2900	**4280**	7410	11600						1560	2900	**4280**	7410	11600
HD 377	00 08 25.75	+06 37 0.49	G2V	0.63	−4.35	150	2,3	69	193	**366**	1200	3620	22	88	**196**	824	5430	55	118	**202**	323	716
HD 375	00 08 28.47	+34 56 4.35	F8	0.61	−4.86		3	2150	3920	**5650**	8720	12100						2150	3920	**5650**	8720	12100
HD 330	00 08 4.69	+53 47 46.50	F8V	0.59		71	4						295	858	**2710**	7670	12000	295	858	**2710**	7670	12000
HD 400	00 08 40.94	+36 37 37.65	F8IV	0.50	−4.80		3	1530	2860	**4220**	7350	11600						1530	2860	**4220**	7350	11600
HD 457	00 08 59.68	−39 44 13.78	G0V	0.62	−4.95		3	3260	5790	**8090**	10500	12600						3260	5790	**8090**	10500	12600
HD 483	00 09 19.44	+17 32 2.12	G2III	0.64	−4.58		3	381	853	**1400**	3430	8930						381	853	**1400**	3430	8930
HD 449	00 09 2.85	+09 50 59.88	G5	0.71	−4.93		3	2970	5310	**7460**	10100	12500						2970	5310	**7460**	10100	12500
HD 531B	00 09 51.30	+08 27 11.89	G7V	0.72	−4.35		3	71	195	**370**	1210	3650						71	195	**370**	1210	3650
HD 531A	00 09 51.65	+08 27 11.40	G6V	0.72	−4.32		3	51	158	**321**	1070	3150						51	158	**321**	1070	3150
HD 531	00 09 51.65	+08 27 11.41	G6V+G7V	0.72	−4.33		3	57	168	**334**	1100	3280						57	168	**334**	1100	3280
HD 564	00 09 52.82	−50 16 4.17	G2/3V	0.59	−4.72		3	1010	1950	**2980**	5860	10900						1010	1950	**2980**	5860	10900
* 6 Cet	00 11 15.85	−15 28 4.74	F8VFe-0.8CH-0.5	0.49	−4.79		3	1500	2790	**4130**	7260	11600						1500	2790	**4130**	7260	11600
V* V344 And	00 11 22.44	+30 26 58.47	K0V	0.76	−4.30		3	43	139	**300**	1000	2910						43	139	**300**	1000	2910
HD 750	00 11 35.79	−57 28 21.18	K1V	0.89	−4.68		3	748	1490	**2330**	4950	10300						748	1490	**2330**	4950	10300
* tet Scl	00 11 44.02	−35 07 59.23	F5V	0.46	−4.64		3	595	1230	**1950**	4360	9830						595	1230	**1950**	4360	9830
BD+64 9	00 12 0.92	+65 36 17.53	F8	0.57		3	4						1790	4840	**8870**	11800	12800	1790	4840	**8870**	11800	12800
HD 804	00 12 28.33	+20 14 3.65	G5	0.67	−4.97		3	3520	6230	**8650**	10900	12600						3520	6230	**8650**	10900	12600
HD 870	00 12 50.25	−57 54 45.40	K0V	0.78	−4.75		3	1200	2280	**3430**	6450	11200						1200	2280	**3430**	6450	11200
HD 984	00 14 10.25	−07 11 56.81	F7V	0.52	−4.34		3	65	184	**354**	1160	3490						65	184	**354**	1160	3490
HD 1108	00 15 4.63	−68 31 48.36	G6V	0.69	−4.80		3	1520	2830	**4190**	7310	11600						1520	2830	**4190**	7310	11600

References—(1) Nielsen & Close (2010), (2) Brandt et al. (2014a), (3) Boro Saikia et al. (2018), (4) Guillout et al. (2009)

Note—RA and Dec from Simbad online services. Table 2 is published in its entirety in machine-readable format.

6. CONCLUSION

We have implemented a Bayesian framework, BAFFLES, for determining the posterior probability density function on stellar age from measurements of R'_{HK} calcium emission and/or $B-V$ color and Li EW lithium abundance. Importantly, BAFFLES properly incorporates astrophysical scatter and physical priors. In developing this framework:

1. We empirically determine the evolution over time of spectral indicators R'_{HK} and Li EW for clusters of stars with well-characterized isochronal ages.

2. Using these benchmark clusters, we derive a numerical likelihood that gives age as a function of R'_{HK} for stars with 0.45 ≤B-V≤ 0.9 and age as a function of $B-V$ and Li EW for 0.35 ≤B-V≤ 1.9.

3. From our tests, the method appears self-consistent and produces robust posteriors on age.

Looking ahead to future space missions, accurate ages become increasingly important. In the next few years *Gaia* is expected to discover thousands of exoplanets and brown dwarfs from measuring precise astrometry of host stars (Perryman et al. 2014). *The James Webb Space Telescope* (JWST), planned to launch in 2021, should be able to survey the nearest and youngest of these *Gaia* targets to directly image the orbiting planets in the thermal infrared, where intermediate age (∼100 Myr - 1 Gyr) planets have more favorable contrasts than the near infrared (Beichman et al. 2019). Likewise the European Extremely Large Telescope (E-ELT) (e.g. Tamai et al. 2016), Thirty Meter Telescope (TMT) (e.g. Simard et al. 2016), and Giant Magellan Telescope (GMT) (e.g. Fanson et al. 2018) will in the near future advance our ability to directly image exoplanets. For the next generation of telescopes, we will need stellar ages to help choose the targets for observing, since for direct imaging younger planets are more luminous and so easier to detect and characterize. Similarly, when exoplanets are discovered the ages of the host stars will allow mass determination for the self-luminous stellar companions. Additionally, significant evolution of planetary systems is predicted over hundreds of Myr (Chiang & Murray 2002; Ford & Rasio 2008; Frelikh et al. 2019), and having a large number of giant planet systems with well-characterized ages will allow these predictions to be directly tested. BAFFLES will fill a unique role in producing robust age posteriors in a uniform way for lower-mass field stars.

We thank Eric Mamajek for helpful conversations that improved this manuscript, and for compiling "The Lithium Plot"[2], which inspired some of this work. This research has made use of the SIMBAD and VizieR databases, operated at CDS, Strasbourg, France. R.D. acknowledges support from the Fonds de Recherche du Québec. Supported by NSF grants AST-1411868 (E.L.N., B.M.), and AST-1518332 (R.D.R.). Supported by NASA grants NNX14AJ80G (E.L.N., B.M.), NNX15AC89G and NNX15AD95G (B.M., R.J.D.R.).

Software: Astropy (Astropy Collaboration et al. 2013), SciPy (Jones et al. 2001–)

[2] http://www.pas.rochester.edu/~emamajek/images/li.jpg

REFERENCES

Allard, F. 2014, in IAU Symposium, Vol. 299, Exploring the Formation and Evolution of Planetary Systems, ed. M. Booth, B. C. Matthews, & J. R. Graham, 271–272

Anthony-Twarog, B. J., Deliyannis, C. P., Harmer, D., et al. 2018, AJ, 156, 37

Arriagada, P. 2011, ApJ, 734, 70

Asiain, R., Figueras, F., Torra, J., & Chen, B. 1999, A&A, 341, 427

Astropy Collaboration, Robitaille, T. P., Tollerud, E. J., et al. 2013, A&A, 558, A33

Balachandran, S. 1995, ApJ, 446, 203

Balachandran, S. C., Mallik, S. V., & Lambert, D. L. 2011, Monthly Notices of the Royal Astronomical Society, 410, 2526

Baliunas, S. L., & Vaughan, A. H. 1985, ARA&A, 23, 379

Baraffe, I., Homeier, D., Allard, F., & Chabrier, G. 2015, A&A, 577, A42

Barnes, S. A. 2009, in IAU Symposium, Vol. 258, The Ages of Stars, ed. E. E. Mamajek, D. R. Soderblom, & R. F. G. Wyse, 345–356

Barrado y Navascués, D., Stauffer, J. R., Hartmann, L., & Balachandran, S. C. 1997, ApJ, 475, 313

Barrado y Navascués, D., Stauffer, J. R., & Jayawardhana, R. 2004, ApJ, 614, 386

Beichman, C., Barrado, D., Belikov, R., et al. 2019, BAAS, 51, 58

Bell, C. P. M., Mamajek, E. E., & Naylor, T. 2015, MNRAS, 454, 593
Boesgaard, A. M., & Tripicco, M. J. 1986, ApJL, 302, L49
Bonfils, X., Delfosse, X., Udry, S., et al. 2013, A&A, 549, A109
Boro Saikia, S., Marvin, C. J., Jeffers, S. V., et al. 2018, A&A, 616, A108
Bowler, B. P. 2016, PASP, 128, 102001
Brandt, T. D., & Huang, C. X. 2015, ApJ, 807, 58
Brandt, T. D., McElwain, M. W., Turner, E. L., et al. 2014a, ApJ, 794, 159
Brandt, T. D., Kuzuhara, M., McElwain, M. W., et al. 2014b, ApJ, 786, 1
Burke, C. J., Pinsonneault, M. H., & Sills, A. 2004, The Astrophysical Journal, 604, 272
Casagrande, L., Schönrich, R., Asplund, M., et al. 2011, A&A, 530, A138
Chiang, E. I., & Murray, N. 2002, ApJ, 576, 473
Choi, J., Dotter, A., Conroy, C., et al. 2016, ApJ, 823, 102
Cummings, J. D., & Kalirai, J. S. 2018, The Astronomical Journal, 156, 165
Cunha, M. S., Aerts, C., Christensen-Dalsgaard, J., et al. 2007, Astronomy and Astrophysics Review, 14, 217
David, T. J., & Hillenbrand, L. A. 2015, ApJ, 804, 146
de Zeeuw, P. T., Hoogerwerf, R., de Bruijne, J. H. J., Brown, A. G. A., & Blaauw, A. 1999, AJ, 117, 354
Delorme, P., Schmidt, T., Bonnefoy, M., et al. 2017, A&A, 608, A79
Donahue, R. A. 1993, PhD thesis, New Mexico State University, University Park.
Duncan, D. K., Vaughan, A. H., Wilson, O. C., et al. 1991, ApJS, 76, 383
Fanson, J., McCarthy, P. J., Bernstein, R., et al. 2018, in Society of Photo-Optical Instrumentation Engineers (SPIE) Conference Series, Vol. 10700, Proc. SPIE, 1070012
Ford, A., Jeffries, R. D., James, D. J., & Barnes, J. R. 2001, A&A, 369, 871
Ford, E. B., & Rasio, F. A. 2008, ApJ, 686, 621
Frelikh, R., Jang, H., Murray-Clay, R. A., & Petrovich, C. 2019, arXiv e-prints, arXiv:1906.03266
Gallet, F., & Bouvier, J. 2013, A&A, 556, A36
Giampapa, M. S., Hall, J. C., Radick, R. R., & Baliunas, S. L. 2006, ApJ, 651, 444
Gossage, S., Conroy, C., Dotter, A., et al. 2018, ApJ, 863, 67
Goudfrooij, P., Girardi, L., Kozhurina-Platais, V., et al. 2014, The Astrophysical Journal, 797, 35
Gray, R. O., Corbally, C. J., Garrison, R. F., et al. 2006, AJ, 132, 161
Guillout, P., Klutsch, A., Frasca, A., et al. 2009, Astronomy and Astrophysics, 504, 829
Hall, J. C., Henry, G. W., Lockwood, G. W., Skiff, B. A., & Saar, S. H. 2009, AJ, 138, 312
Henry, T. J., Soderblom, D. R., Donahue, R. A., & Baliunas, S. L. 1996, AJ, 111, 439
Høg, E., Fabricius, C., Makarov, V. V., et al. 2000, A&A, 355, L27
Isaacson, H., & Fischer, D. 2010, ApJ, 725, 875
Jenkins, J. S., Jones, H. R. A., Tinney, C. G., et al. 2006, MNRAS, 372, 163
Jones, B. F., Fischer, D., Shetrone, M., & Soderblom, D. R. 1997, AJ, 114, 352
Jones, B. F., Fischer, D., & Soderblom, D. R. 1999, AJ, 117, 330
Jones, E., Oliphant, T., Peterson, P., et al. 2001–, SciPy: Open source scientific tools for Python, [Online; accessed ¡today¿]
King, J. R. 1998, AJ, 116, 254
King, J. R., & Schuler, S. C. 2005, PASP, 117, 911
King, J. R., Villarreal, A. R., Soderblom, D. R., Gulliver, A. F., & Adelman, S. J. 2003, AJ, 125, 1980
Konopacky, Q. M., Rameau, J., Duchêne, G., et al. 2016, ApJL, 829, L4
Kraft, R. P. 1967, ApJ, 150, 551
Lachaume, R., Dominik, C., Lanz, T., & Habing, H. J. 1999, A&A, 348, 897
Lovis, C., Dumusque, X., Santos, N. C., et al. 2011, arXiv e-prints, arXiv:1107.5325
Macintosh, B., Chilcote, J. K., Bailey, V. P., et al. 2018, in Society of Photo-Optical Instrumentation Engineers (SPIE) Conference Series, Vol. 10703, Adaptive Optics Systems VI, 107030K
Makarov, V. V. 2006, AJ, 131, 2967
Mamajek, E. E. 2012, ApJL, 754, L20
Mamajek, E. E., & Hillenbrand, L. A. 2008, ApJ, 687, 1264
Mamajek, E. E., Meyer, M. R., & Liebert, J. 2002, AJ, 124, 1670
Meibom, S., Mathieu, R. D., Stassun, K. G., Liebesny, P., & Saar, S. H. 2011, ApJ, 733, 115
Mentuch, E., Brandeker, A., van Kerkwijk, M. H., Jayawardhana, R., & Hauschildt, P. H. 2008, ApJ, 689, 1127
Mesa, D., Baudino, J. L., Charnay, B., et al. 2018, A&A, 612, A92
Milli, J., Hibon, P., Christiaens, V., et al. 2017, A&A, 597, L2
Nielsen, E. L., & Close, L. M. 2010, ApJ, 717, 878
Nielsen, E. L., Liu, M. C., Wahhaj, Z., et al. 2013, ApJ, 776, 4

Nielsen, E. L., De Rosa, R. J., Macintosh, B., et al. 2019, arXiv e-prints, arXiv:1904.05358

Noyes, R. W., Hartmann, L. W., Baliunas, S. L., Duncan, D. K., & Vaughan, A. H. 1984, ApJ, 279, 763

Pace, G. 2013, A&A, 551, L8

Pace, G., Castro, M., Melendez, M., Theado, S., & Do Nascimento, Jr., J.-D. 2012, VizieR Online Data Catalog, 354

Pecaut, M. J., & Mamajek, E. E. 2013, ApJS, 208, 9

—. 2016, MNRAS, 461, 794

Perryman, M., Hartman, J., Bakos, G. Á., & Lindegren, L. 2014, ApJ, 797, 14

Randich, S., Pallavicini, R., Meola, G., Stauffer, J. R., & Balachandran, S. C. 2001, VizieR Online Data Catalog, 337

Randich, S., Tognelli, E., Jackson, R., et al. 2018, A&A, 612, A99

Sestito, P., & Randich, S. 2005, A&A, 442, 615

Shkolnik, E. L., Allers, K. N., Kraus, A. L., Liu, M. C., & Flagg, L. 2017, AJ, 154, 69

Simard, L., Ellerbroek, B., Bhatia, R., Radovan, M., & Chisholm, E. 2016, in Society of Photo-Optical Instrumentation Engineers (SPIE) Conference Series, Vol. 9908, Proc. SPIE, 99081V

Skumanich, A. 1971, in BAAS, Vol. 3, Bulletin of the American Astronomical Society, 455

Snaith, O., Haywood, M., Di Matteo, P., et al. 2015, A&A, 578, A87

Soderblom, D. R. 2010, ARA&A, 48, 581

Soderblom, D. R., Duncan, D. K., & Johnson, D. R. H. 1991, ApJ, 375, 722

Soderblom, D. R., Jones, B. F., Balachandran, S., et al. 1993, AJ, 106, 1059

Soderblom, D. R., Oey, M. S., Johnson, D. R. H., & Stone, R. P. S. 1990, AJ, 99, 595

Sung, H., & Bessell, M. S. 1999, MNRAS, 306, 361

Talon, S., & Charbonnel, C. 2010, in IAU Symposium, Vol. 268, Light Elements in the Universe, ed. C. Charbonnel, M. Tosi, F. Primas, & C. Chiappini, 365–374

Tamai, R., Cirasuolo, M., González, J. C., Koehler, B., & Tuti, M. 2016, in Society of Photo-Optical Instrumentation Engineers (SPIE) Conference Series, Vol. 9906, Proc. SPIE, 99060W

Tobin, J. J., Hartmann, L., Fűrész, G., Hsu, W.-H., & Mateo, M. 2015, AJ, 149, 119

Turner, D. G. 2012, Astronomische Nachrichten, 333, 174

VandenBerg, D. A., & Stetson, P. B. 2004, PASP, 116, 997

Weber, E. J., & Davis, Jr., L. 1967, ApJ, 148, 217

Wright, J. T., Marcy, G. W., Butler, R. P., & Vogt, S. S. 2004, ApJS, 152, 261

Zapatero Osorio, M. R., Béjar, V. J. S., Pavlenko, Y., et al. 2002, A&A, 384, 937